J Appl Physiol 127: 1328–1337, 2019.
First published September 12, 2019; doi:10.1152/japplphysiol.00324.2019.

INNOVATIVE METHODOLOGY

Diffuse correlation spectroscopy and frequency-domain near-infrared spectroscopy for measuring microvascular blood flow in dynamically exercising human muscles

Valentina Quaresima,[1]* Parisa Farzam,[2]* Pamela Anderson,[3] Parya Y. Farzam,[2] Daniel Wiese,[3] Stefan A. Carp,[2] Marco Ferrari,[1] and Maria Angela Franceschini[2]

[1]*Department of Life, Health and Environmental Sciences, University of L'Aquila, L'Aquila, Italy;* [2]*Optics at Athinoula A. Martinos Center for Biomedical Imaging, Massachusetts General Hospital, Harvard Medical School, Charlestown, Massachusetts; and* [3]*Dynometrics, Cambridge, Massachusetts*

Submitted 10 May 2019; accepted in final form 5 September 2019

Quaresima V, Farzam P, Anderson P, Farzam PY, Wiese D, Carp SA, Ferrari M, Franceschini MA. Diffuse correlation spectroscopy and frequency-domain near-infrared spectroscopy for measuring microvascular blood flow in dynamically exercising human muscles. *J Appl Physiol* 127: 1328–1337, 2019. First published September 12, 2019; doi:10.1152/japplphysiol.00324.2019.—In the last 20 yr, near-infrared diffuse correlation spectroscopy (DCS) has been developed for providing a noninvasive estimate of microvascular blood flow (BF) as a BF index (BF_i) in the human skin, muscle, breast, brain, and other tissue types. In this study, we proposed a new motion correction algorithm for DCS-derived BF_i able to remove motion artifacts during cycling exercise. We tested this algorithm on DCS data collected during cycling exercise and demonstrated that DCS can be used to quantify muscle BF_i during dynamic high-intensity exercise. In addition, we measured tissue regional oxygen metabolic rate (MRO_{2i}) by combining frequency-domain multidistance near-infrared spectroscopy (FDNIRS) oximetry with DCS flow measures. Recreationally active subjects ($n = 12$; 31 ± 8 yr, 183 ± 4 cm, 79 ± 10 kg) pedaled at 80–100 revolutions/min until volitional fatigue with a work rate increase of 30 W every 4 min. Exercise intensity was normalized in each subject to the cycling power peak (W_{peak}). Both rectus femoris BF_i and MRO_{2i} increased from 15% up to 75% W_{peak} and then plateaued to the end of the exercise. During the recovery at 30 W cycling power, BF_i remained almost constant, whereas MRO_{2i} started to decrease. The BF_i/MRO_{2i} plateau was associated with the rising of the lactate concentration, indicating the progressive involvement of the anaerobic metabolism. These findings further highlight the utility of DCS and FDNIRS oximetry as effective, reproducible, and noninvasive techniques to assess muscle BF_i and MRO_{2i} in real time during a dynamic exercise such as cycling.

NEW & NOTEWORTHY To the best of our knowledge, this study is the first to demonstrate that diffuse correlation spectroscopy in combination with frequency-domain near-infrared spectroscopy can monitor human quadriceps microvascular blood flow and oxygen metabolism with high temporal resolution during a cycling exercise. The optically measured parameters confirm the expected relationship between blood flow, muscle oxidative metabolism, and lactate production during exercise.

blood flow; diffuse correlation spectroscopy; exercise; muscle oxidative metabolism; near-infrared spectroscopy

INTRODUCTION

Previous studies on the regulation of skeletal muscle blood flow (BF) during exercise in humans (32) have been severely limited by the lack of high-temporal-resolution methods for the continuous, precise determination of muscle BF at the microcirculatory level (19). Such methods would provide a better understanding of regional muscle BF regulation. Although contrast-enhanced ultrasound has the potential to estimate overall microcirculatory BF, this method cannot be applied during dynamic high-intensity muscle exercise (19). Since the end of the 1980s, near-infrared spectroscopy (NIRS) has been utilized to investigate local muscle oxidative metabolism at rest and during different exercise modalities. One of the key advantages of using NIRS is that its signals can yield acceptable signal-to-noise ratios even during dynamic exercise. Detailed NIRS reviews have been published on the methodology (also known as tissue oximetry), the medical/sports sciences applications, and its potential limitations (3, 17, 23, 34). Recently, the review by Grassi and Quaresima (20) from an "exercise physiology point of view" was devoted to discussing some of the main issues relating to the role of NIRS in the functional assessment of oxidative metabolism in skeletal muscles during exercise, with specific attention to integrative aspects and to the factors limiting exercise tolerance. In the last 20 years a complementary optical technique, near-infrared diffuse correlation spectroscopy (DCS), has been developed for the continuous measurement of BF in tissue. Applications to human skeletal muscle, breast cancer, and the brain cortex (11, 27, 37) have been demonstrated. DCS uses the temporal fluctuations of diffusely reflected light to quantify the motion of moving scatterers, which in tissue is dominated by the motion of red blood cells; DCS provides a noninvasive estimate of deep tissue microvascular BF as a BF index (BF_i) with units cm^2/s. DCS-derived BF_i has been validated against established muscle perfusion measurement methods, specifically arterial spin labeling MRI in human calf (41) and fluorescent microspheres in murine quadriceps (35). DCS-derived BF_i has also been recently validated in humans with Doppler ultrasound during a

* V. Quaresima and P. Farzam are co-first authors.

Address for reprint requests and other correspondence: V. Quaresima, Dept. of Life, Health and Environmental Sciences, Univ. of L'Aquila, 67100 L'Aquila, Italy (e-mail: valentina.quaresima@univaq.it).

rhythmic handgrip exercise (2, 39) demonstrating that DCS-derived BF_i is more reliable and less susceptible to motion artifacts than Doppler ultrasound. By combining oximetry and DCS flow measures, the tissue regional oxygen metabolic rate (MRO_{2i}), a parameter closely linked to underlying physiology and pathological states, can be quantified (11, 36). The MRO_{2i} is an important parameter that has been investigated in the human newborn brain, given the strong dependence of this organ on aerobic metabolism (15, 16). Very recently, the first device combining frequency-domain multidistance NIRS (FDNIRS) and DCS technologies has become commercially available; this instrument, described in Ref. 7, is capable of measuring the absolute concentrations of deoxygenated-hemoglobin (deoxy[Hb+Mb]), oxygenated-hemoglobin (oxy[Hb+Mb]), total hemoglobin (total[Hb+Mb]), and hemoglobin oxygen saturation (StO_2; %) as well as BF_i and MRO_{2i}. The same quantities can be measured in newborns by a recent commercially available system that combines time-domain NIRS and DCS (1, 18). Regarding the application of the hybrid FDNIRS-DCS system for human skeletal muscle studies, so far, the instrument has been utilized only to measure relative BF_i changes in flexor digitorum superficialis muscle BF during the 10-s end-stage resting periods of exercise of varying power (24). In the latter (24) and in most of the prior studies (utilizing noncommercial devices), recently reviewed by Hou et al. (27), DCS has never been used continuously during dynamic exercise because of the large motion artifacts inherent to the DCS method, which mask the motion of the red blood cells. In fact, previous works have limited BF_i analysis to short intervals during the exercise, in which the muscle is not contracted and not moving, or during plantar flexion exercise (21, 38). In this study, we propose a new empirical model that is able to compensate for the motion artifacts and muscle fibers contractions, allowing us to recover BF_i continuously during dynamic cycling exercise.

Concerning the time course of muscle BF during human incremental exercises, a plateauing of microvascular BF at submaximal work rates in the quadriceps [over 60% cycling power peak (W_{peak})] and in the flexor digitorum superficialis (over 66% W_{peak}) were found in the studies using either the invasive indocyanine green method and NIRS (22) or the noninvasive DCS approach (24), respectively.

The aims of this study were to *1*) provide, for the first time to the best of our knowledge, a proof of concept demonstration of the feasibility of DCS-derived BF_i measurement during dynamic high-intensity muscle exercise using a motion correction algorithm; *2*) compare muscle and subcutaneous BF changes induced by a dynamic exercise; and *3*) combine DCS-derived BF_i and FDNIRS oximetry + DCS-derived MRO_{2i} measurements on the right superficial rectus femoris during a ramp-incremental cycling exercise until volitional fatigue. We hypothesized that BF_i and MRO_{2i} would increase with increasing exercise intensity and would plateau at a submaximal work rate. The relationship between BF_i and MRO_{2i} with lactate production was also investigated. Limitations and assumptions of the present study are discussed.

METHODS

Participants. Eighteen recreationally active subjects were enrolled. Enrollment criteria included practicing endurance training at least 3 times a week (~40 min each time at moderate intensity) and excluded subjects with any knee instability or chronic conditions, including heart or respiratory disorder, smoking, or substance abuse. The study protocol was reviewed and approved by the Institutional Review Board for Partners Healthcare, the Partners Human Research Committee. The study method was designed and carried out in accordance with the Partners Human Research Committee requirements and the regulations that govern human subjects research in compliance with the latest version of the Declaration of Helsinki. Each participant gave written informed consent to participate in the study. All the participants were familiar with the testing protocols and were instructed to abstain from caffeine, alcohol, and intensive physical exercise for 24 h before the experimental procedure. The experimental protocol consisted of performing a ramp-incremental test on an electronically braked cycle ergometer (Model E3, Kettler, Germany). Before beginning the protocol, basic information was collected for each subject. This information included age, height, weight, and sex. Body mass index was calculated and expressed as kilograms per square meter. Subcutaneous adipose tissue thickness (ATT) over the superficial rectus femoris was measured using a skinfold caliper. Peripheral arterial oxygen saturation (SpO_2) and hemoglobin level (HGB) were measured by a pulse CO-oximeter (Rad-87, Masimo, Irvine, CA). Body temperature was measured using a noncontact thermometer (CVS Health Rigid Tip Digital Thermometer) before the incremental ramp test. In addition, each subject wore a heart rate (HR) monitor strap (Polar Electro Oy, Kempele, Finland) around the chest to record HR continuously during the test. Supplementary Table S1 summarizes the anthropometrics and physiological measures of the 18 subjects (all Supplemental Material is available at https://doi.org/10.6084/m9.figshare.8101103).

Experimental protocol. Each subject performed a ramp-incremental cycling exercise. A fiber-optics probe, connected to the FDNIRS-DCS device, was positioned over the belly of the right superficial rectus femoris using tissue palpations (Fig. 1). The probe was attached to the skin with a transparent film dressing and was secured around the thigh using a black self-adherent wrap bandage. The accuracy of the contact between the probe and the skin was verified at the end of the protocol (i.e., slightly depressed cutaneous area corresponding to the location of probe). Although both the vastus lateralis and rectus femoris are dominant locomotor muscle groups during cycling, the rectus femoris was chosen to minimize optical fiber movement throughout the exercise. The two muscle groups, however, do have different fiber-type composition and have different electromyogram activation patterns during maximal ramp exercise (8). The scheme of the adopted protocol is shown in Fig. 1. The ramp protocol consisted of a 2-min rest on the bike, then a 4-min warm up at 30 W, followed by a 30-W incremental ramp. The subjects were instructed to maintain a constant pace of ~80–100 revolutions/min throughout the entire exercise. According to the Internal Review Board recommendation, the subjects were informed to ask for the interruption of the protocol as soon as they were unable to maintain the pedal cadence (80–100 revolutions/min) and/or they felt tired. Considering that the subjects were recreationally active with a heterogeneous performance, it was expected that everyone, independently of the sex, could be able to achieve a W_{peak} of at least 210 W. This threshold was chosen a priori considering that several previous studies demonstrated that quadriceps BF increases during the ramp cycling exercise and plateaus at submaximal exercise (200–220 W) (22). Among the 18 subjects, only 12 male subjects were considered in the study because they were able to reach or pass this threshold (age: 31 ± 8 yr; weight: 79 ± 10 kg; height: 183 ± 4 cm) (Supplemental Table S1 and Fig. S1).

At the limit of the tolerance, the bike power was set to 30 W for 4 min. The recording ended after a 2-min rest with no pedaling. Cycling power peak (W_{peak}) was determined as the power output during the final stage of exercise lasting a minimum of 1.5 min. During the last 30 s of each interval, a small pinprick blood sample was taken from the fingertip to measure the lactate concentration (Lactate Plus Meter, Nova Biomedical, Waltham, MA). Two readings were repeated at each interval.

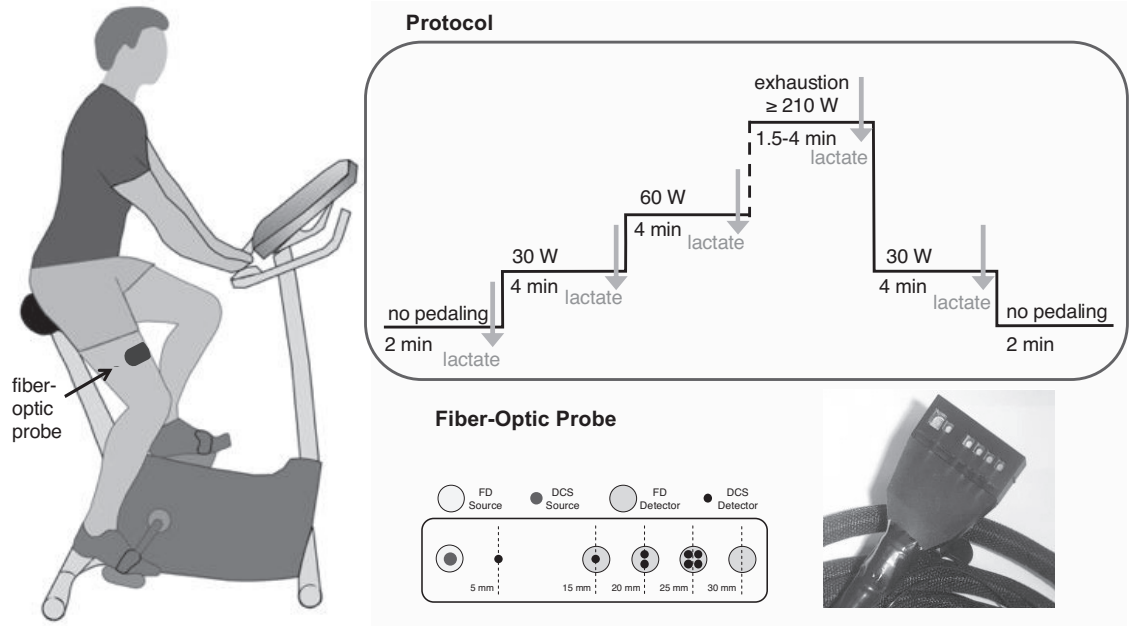

Fig. 1. *Left*: drawing of a subject cycling on a stationary bicycle with a frequency-domain (FD) multidistance near-infrared spectroscopy (FDNIRS)-diffuse correlation spectroscopy (DCS) probe attached to the right superficial rectus femoris. *Top right*: schematic diagram of the measurement protocol. The power was increased by 30 W at the end of each 4-min cycling step. During the last 30 s of each step, a small pinprick blood sample was taken from the fingertip to measure the lactate concentration. *Bottom right*: drawing of fiber-optic probe geometry and photograph of the probe. In the drawing the larger and lighter-gray circles indicate the FDNIRS components, and the smaller and darker-color circles indicate the DCS components. The FDNIRS detectors are located at 15, 20, 25, and 30 mm from the source. The DCS detectors are at 5, 15, 20, and 25 mm from the source. An additional 2–4 fibers (1 per detector) were included to increase the DCS signal-to-noise ratio at larger separations (20 and 25 mm).

FDNIRS-DCS instrumentation. A hybrid system, equipped to employ FDNIRS and DCS, was used to measure superficial rectus femoris hemodynamics and oxidative metabolism during the ramp-incremental cycling exercise (MetaOx, ISS Inc., Champaign, IL). A detailed description of this device can be found elsewhere (7, 24). The FDNIRS component includes 1 source channel with 8 time-shared diode laser-emitting light at different wavelengths (from 670 to 830 nm) and 4 photomultiplier detector channels. The DCS component includes 1 long coherence length solid-state laser at 850 nm and 8 photon-counting detectors. The 2 modalities are acquired simultaneously at 10 Hz to provide and display in real-time oxy[Hb+Mb], deoxy[Hb+Mb], total[Hb+Mb], StO_2, BF_i, and MRO_{2i} (7). The light from the FDNIRS and DCS components is delivered to the tissue via optical fibers with a custom three-dimensional printed probe (Fig. 1). At the probe end, source and detectors of the 2 modalities are combined with the small DCS fibers (5.6-μm core diameter single-mode fibers for the detectors, 100-μm core diameter multimode fiber for the source) at the center of the larger FDNIRS fiber bundles (2.5-mm diameter multimode fiber bundles) and terminated with glass prisms to direct the light perpendicularly toward the tissue and maintain a low profile as described in Ref. 5. The fibers are distributed in a row with the FDNIRS detectors located at 15, 20, 25, and 30 mm from the source and the DCS detector fibers located at 5, 15, 20, and 25 mm from the source, increasing the number of detectors at larger separations to improve signal-to-noise ratio. The probe, shown in Fig. 1, is very light and measures 4.5 × 2 × 0.8 mL.

Data analysis. The details of the FDNIRS data analysis have been previously described (15). In brief, the multidistance FDNIRS method was used to recover the tissue optical properties (absorption and reduced scattering coefficients, μ_a and μ'_s, respectively) at the 8 wavelengths (14), and deoxy[Hb+Mb], oxy[Hb+Mb], total[Hb+Mb], and StO_2 were derived from the absorption spectra assuming a 75% tissue water concentration. StO_2 reflects the oxygenation of a mixture of arterial and venous blood, with a higher contribution from the capillaries (20). To estimate BF_i from the DCS data, we derived the temporal intensity autocorrelation function (g_2) at each source-detector separation and used the semi-infinite homogeneous medium solution to the correlation diffusion equation to fit the autocorrelation curves and estimate the BF_i (12). FDNIRS AC amplitude and phase values and DCS intensity autocorrelations were acquired with a 100-ms temporal resolution. However, to minimize noise and motion artifacts, all the derived parameters were calculated by applying a moving average of 100 points (10 s) [by using the "smooth" function of MATLAB (MathWorks, Natick, MA) programs] and then downsampled to 5 s. For the BF_i calculations, we used the μ_a and μ'_s at 850 nm estimated by extrapolating the spectra obtained with FDNIRS. In addition, to further reduce motion artifacts, we applied the motion correction method described in the next section. We used the DCS measures at 5 mm to evaluate subcutaneous BF_i ($ssBF_i$). For the muscle BF_i, we considered the DCS measures at larger source-detector separations. To minimize partial volume effect because of differences in depth penetration, we considered BF_i at 15-mm and at 20–25-mm depth from the surface in subjects with ATT lower than 4 mm and higher than 4 mm, respectively. In subject 9, although his ATT was higher than 4 mm, we had to use BF_i at 15 mm because of the low photon count rate at larger separations. In all cases, we verified that BF_i temporal changes measured during exercise at 1.5-, 2.0-, and 2.5-cm separations were consistent with each other, the only difference being larger absolute BF_i values at larger separations because of the greater contribution of the muscle tissue compared with the one from the subcutaneous adipose tissue layer. Finally, as done previously (13), using the Fick's principle, we estimated the MRO_{2i} as: $MRO_{2i} = HGB \times BF_i \times (SpO_2 - StO_2)/(0.75 \times$ molecular weight of hemoglobin) (10) from the time-varying BF_i and StO_2, with HGB and SpO_2 measured by pulse oximetry before starting the exercise, the molecular weight of hemoglobin (64,458 g/mol), and the venous ratio correction for StO_2 being 0.75 (29). For the averages across subjects, in each subject at every level we averaged the final 1.5–2 min of data. Since the maximum power reached by each subject has differed, to obtain the same number of power levels on all subjects, exercise

intensity was normalized to the W_{peak} (33), and for each subject only levels close (up to ± 5% difference) to 0%, 15%, 30%, 45%, 60%, 75%, 90%, 100%, 15%, and 0% W_{peak} were considered.

Removing motion artifacts from DCS data. DCS is sensitive to the displacement (movement) of the red blood cells over different timescales (from ns to ms). During exercise, cell movement is due to the additive combination of BF and body movement; the contribution of the latter is an order of magnitude larger than BF (Fig. 2). As it can be seen in Fig. 2, at the onset of pedaling there is a large jump in the uncorrected BF_i because of the pedaling-induced bulk body movement that needs to be compensated for to be able to accurately quantify tissue BF during exercise. The effect of pedaling motion is also seen as an oscillation in the FDNIRS AC amplitude, and it can be used to determine the real-time pedaling rate as described below. We hypothesized that these two components could be modeled as additive, and they could be isolated by independently measuring the subject's movement speed or, more precisely, the pedaling rate. Some cycle ergometers provide the pedaling rate; unfortunately, this wasn't the case of the cycle ergometer adopted for this study. Hence, the pedaling rate was calculated using the oscillatory signal in the FDNIRS data. Specifically, a 20-s Fourier transform was applied to the normalized FDNIRS amplitude (AC), measured at 10 Hz at 1 of the 8 wavelengths; for each interval, a 15-s overlap with the previous interval was used to obtain a cycling rate value every 5 s. Supplemental Fig. S2 shows an example of Fourier transform and estimated cycling frequency for a representative subject. To correct for the pedaling motion artifact and the muscle fibers contractions, we introduced an additional term in the DCS scattering particle displacement expression. For stationary subjects, the scattering particle displacement is typically modeled as $<\Delta r^2(\tau)> = 6BF_i\tau$ (7), where BF_i is the DCS BF index (the effective diffusion coefficient) and τ is the correlation time delay. We modified this equation by adding a term proportional to the pedaling rate and tested two possible empirical models: random walk $<\Delta r^2(\tau)> = 6BF_i\tau + K_D P_r \tau$ and linear motion $<\Delta r^2(\tau)> = 6BF_i\tau + K_V P_r \tau^2$, where P_r is the pedaling rate. K_D and K_V are subject-dependent scaling factors determined from the BF_i change at the onset of the ramp-incremental exercise with a 30-W load. Specifically, their values are calculated by solving the equation resulting from the requirement that the average corrected BF_i value immediately after motion onset (the first 20 s during the 30-W load phase) matches the BF_i value right before motion onset (the last 20-s baseline BF_i). We found that the correction using the random walk term better minimizes the large artifacts because of changes in pedaling rate throughout the exercise and at the end of the exercise when subjects stop pedaling. In addition, for the random walk model, the same K_D can be used to remove motion artifacts at all source-detector separations, whereas K_V changes substantially with source-detector separation. As a result, in our data analysis, this random walk correction model was used. Taking advantage of the linearity of the root mean square displacement with τ, the corrected BF index (BF_{icorr}) was computed simply as $BF_{icorr} = BF_i - K_D P_r$.

Statistical analysis. All statistical analyses were conducted using SPSS 20.0 (SPSS Inc., Chicago, IL). Descriptive data are presented as means ± SD unless otherwise noted. Oxy[Hb+Mb], deoxy [Hb+Mb], total[Hb+Mb], StO_2, BF_i, $ssBF_i$, and MRO_{2i} (calculated as the mean of the last 2 min before the start of the exercise and the last 2 min of each step shown in Fig. 2) were compared across work rates using one-way repeated measures analyses of variance. When a significant overall effect was found, a Tukey post hoc analysis was performed to determine where significant differences existed. Statistical significance was defined as $P < 0.05$. A plateau was

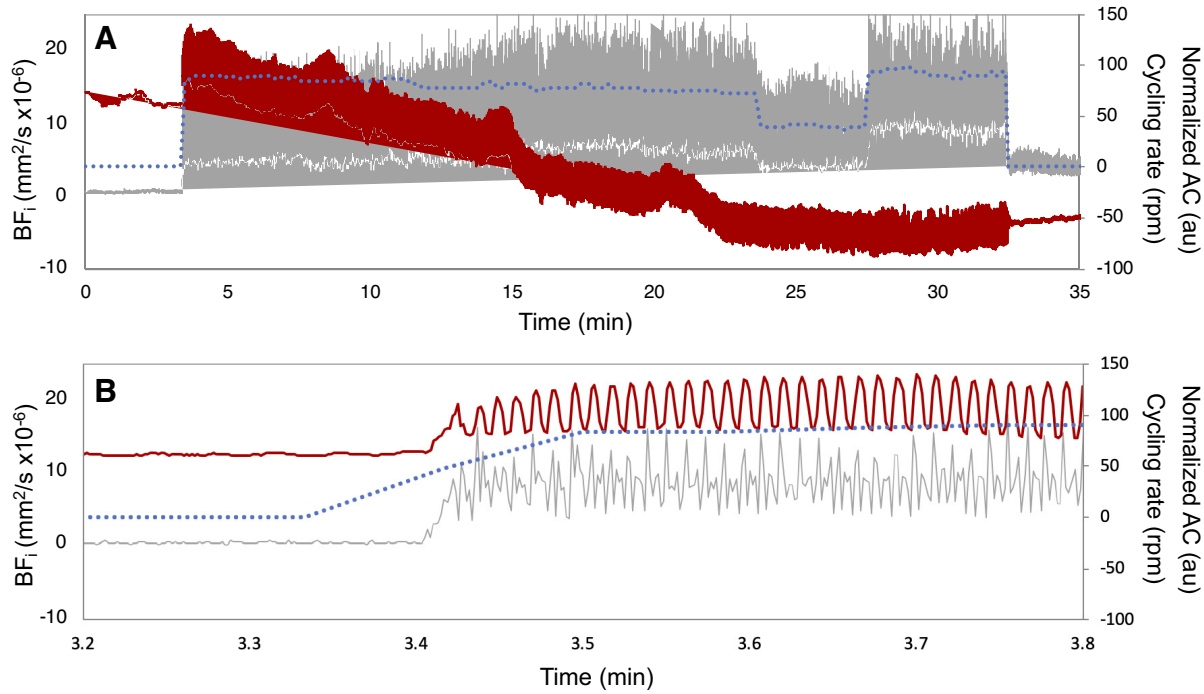

Fig. 2. Diffuse correlation spectroscopy blood flow index (BF_i) before correction (gray), frequency-domain multidistance near-infrared spectroscopy-normalized amplitude (AC; red) measured at 706 nm, acquired at 10 Hz and 2-cm source-detector separation during the whole exercise (*top* graph), and detail at the onset of pedaling (*bottom* graph) on a representative subject (subject 13). The estimated cycling rate from the AC oscillations are shown in blue. The periods of no pedaling at the beginning and at the end of the measurement are distinguishable because of absence of cycling-induced AC and BF_i oscillations. The motion-induced oscillations of the AC signal are much smaller than in the BF_i. The oscillations in the AC signal are periodic, with each period corresponding to a pedaling cycle. Their amplitude is independent of the pedaling rate and minimally affects the mean AC changes because of exercise. The motion artifacts in the BF_i are much more extensive, are not sinusoidal, and are strongly dependent on the pedaling rate, as shown at around 23 min, at which point the subject suddenly slows down. au, arbitrary units.

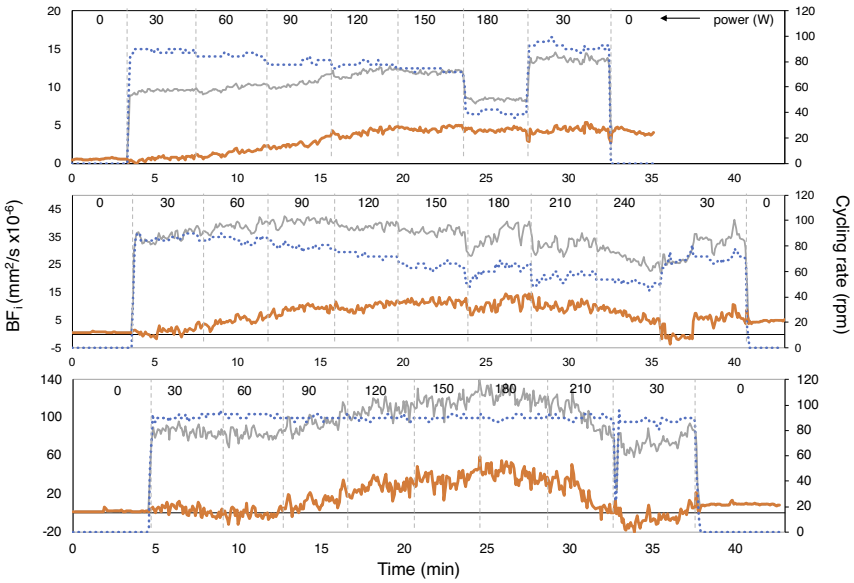

Fig. 3. Noncorrected blood flow index (BF_i; gray line) and corrected BF_i (orange line) rectus femoris blood flow estimates during the ramp-incremental cycle exercise in 3 representative subjects: subject 13 (*top*, excluded from group average), subject 5 (*middle*), and subject 18 (*bottom*). The figure also reports the cycling power levels (*top* black numbers) and the pedaling rates (blue dashed line; *right* *y*-axis).

considered present in a response when a minimum of two consecutive work rate transitions elicited no significant increase.

RESULTS

Figure 3 shows the BF_i (downsampled to 0.2 Hz) before (BF_{inc}; gray line) and after (BF_{icorr}; orange line) random walk model correction for three representative subjects. Subject 13 couldn't keep the pedaling rate at 180 W and terminated the exercise before reaching 210 W. This subject (excluded from the averaged results) had dramatic changes in pedaling rate at the power level of 180 W. This case helps to demonstrate the efficiency of the correction model on recovering artifact-free BF_i. In subject 5 (who couldn't keep the pedaling rate over the last part of the exercise), the noncorrected BF_i decreased during the exercise, whereas, as it was expected, BF_{icorr} increased because of the increased metabolic demand. In subject 18 (who was able to maintain a constant pedaling rate), the BF_i correction shifted the *y*-axis. The random walk model correction, across all 18 measured subjects, consistently has minimized the non-physiological "jumps" when subjects changed the pedaling rate and/or stop pedaling. In a few instances, including subjects 5 and 18 shown in Fig. 3, the correction algorithm has overcompensated, producing slightly negative BF_i values during the recovery phase (30 W). Figure 4 depicts the response of StO_2, $ssBF_i$, BF_i, and MRO_{2i} versus time, measured by the FDNIRS-DCS instrumentation, during the

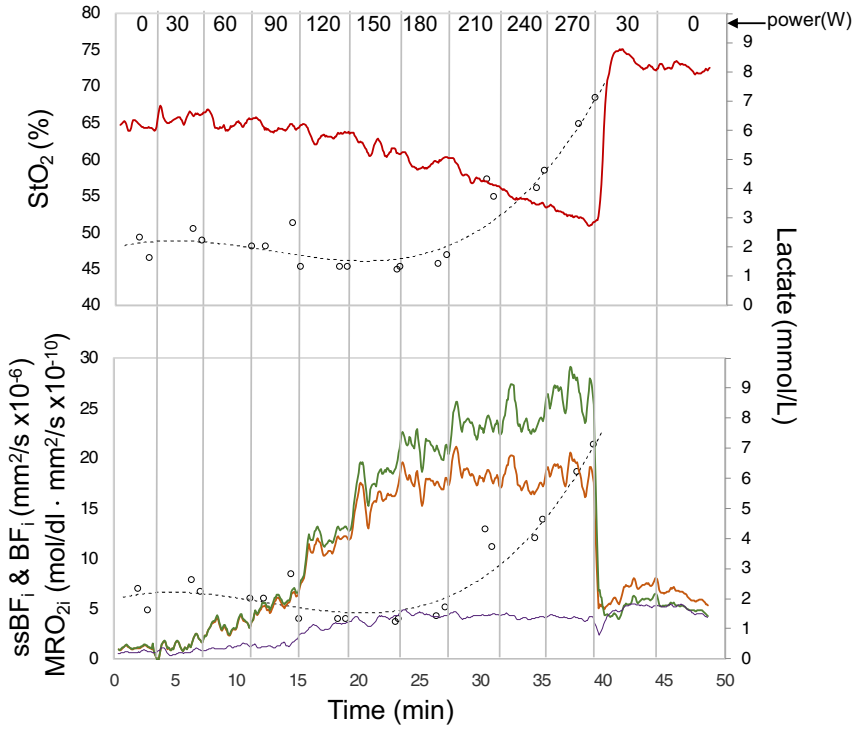

Fig. 4. Rectus femoris hemoglobin oxygen saturation (StO_2; red), muscle blood flow index (BF_i; orange), subcutaneous blood flow index ($ssBF_i$; purple), and tissue regional oxygen metabolic rate (MRO_{2i}; green) for a representative subject (subject 12) during the ramp-incremental cycling exercise. The continuous lines are moving averages over 25 s. Finger-stick capillary blood lactate (black circles); each circle is an average of 2 measurements. The lactate dashed line is a three-order polynomial fit. Note that no increase was observed in BF_i above 150 W. StO_2 overshot immediately when the power was drastically reduced from 270 W to 30 W. At the end of the recovery phase, both BFi and ssBFi were higher than their values observed at the baseline.

entire protocol on a representative subject (subject 12). StO_2 decreased with the increasing of the bike power level and promptly recovered (when switching from 270 to 30 W) to reach values higher than those measured at the pre-exercise time. BF_i and MRO_{2i} increased significantly from baseline values as the cycling power was increasing. When the power level was approaching 150 W (~60% W_{peak}), BF_i plateaued, followed by a plateau of MRO_{2i}. The BF_i plateau was found to be associated with the rise of lactate concentration. The $ssBF_i$ also increased as the cycling power increased and plateaued when lactate concentration was starting to increase. As expected, the $ssBF_i$ increase was substantially lower (77%) than the BF_i increase in the muscle. However, this $ssBF_i$ increase was found significant, and its general trend was similar to the trend of the BF_i increase in the muscle. During the recovery, BF_i and MRO_{2i} promptly dropped to their corresponding values that were observed at the load between 90 and 120 W, whereas $ssBF_i$ further increased with respect to the value found at the last step of the ramp exercise. At the end of the recovery phase, both BF_i and ssBFi were higher than their values observed at the baseline; in addition, BF_i was found higher than ssBFi. The still-high BF_i and ssBFi values during the recovery phase are explainable by the need to satisfy the muscle postexercise increased metabolic demand (30) and the heat dissipation, respectively.

By design, participants achieved different W_{peak} levels, with an average W_{peak} of 242 ± 24 W (Supplemental Fig. S1 and Supplemental Table S1). To obtain averages across subjects, only levels close (up to ± 5% difference) to 0%, 15%, 30%, 45%, 60%, 75%, 90%, and 100% W_{peak} were considered. Figure 5 displays the group mean profiles of the finger-stick capillary blood lactate, HR, StO_2, total[Hb+Mb], BF_i, and MRO_{2i} of the right superficial rectus femoris during the ramp-incremental cycling exercise averaging the last 1.5–2 min of each power level. The HR, as expected, progressively increased up to W_{peak}; blood lactate remained constant for the first few intervals and started to increase around 60% W_{peak}. Similarly, StO_2 remained quite constant until 60% W_{peak} and then started to decrease with the increasing of the power. Nevertheless, only StO_2 at W_{peak} was significantly different from the pre-exercise level. At the end of the exercise, StO_2 promptly recovered, reaching the pre-exercise values; total [Hb+Mb] increased over the interval 15%–60% W_{peak} and plateaued at above 60% W_{peak}. The large error bars of total[Hb+Mb] values are due to the large intersubject variability of the hemoglobin concentration. Both rectus femoris BF_i

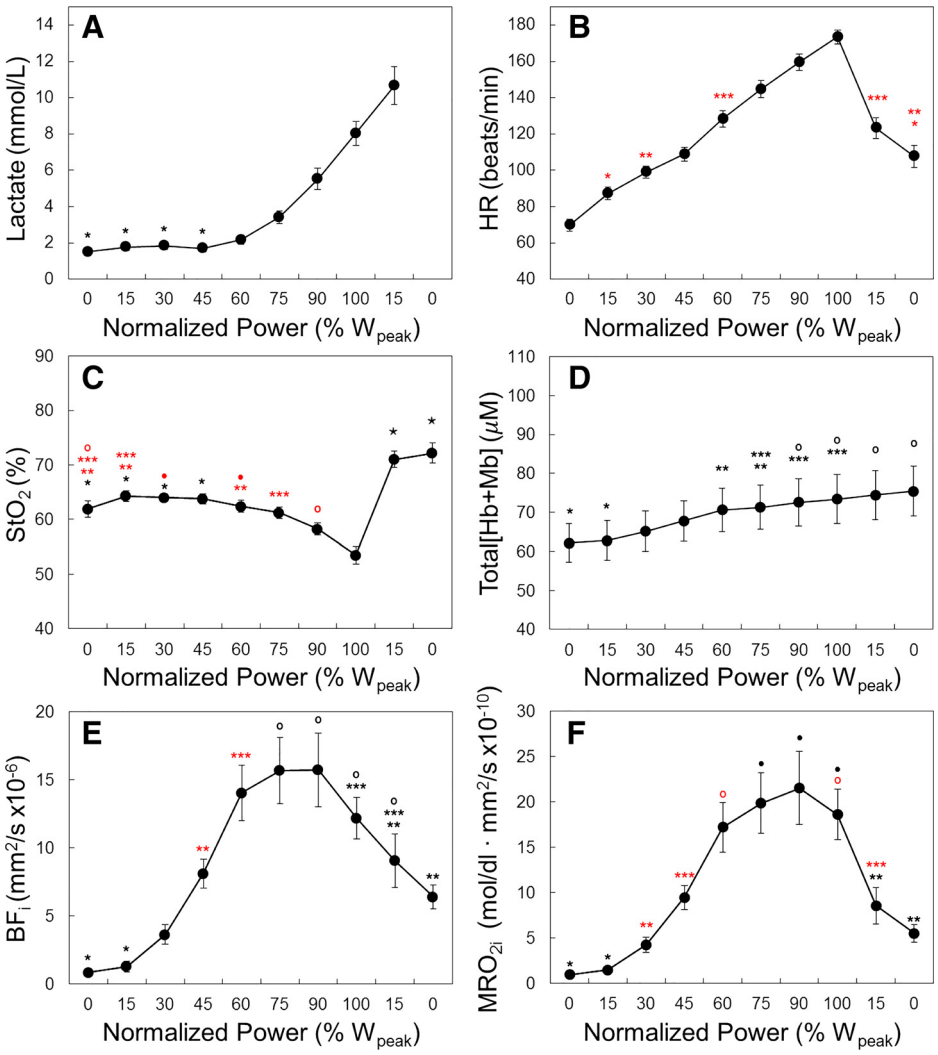

Fig. 5. Group mean profiles of the finger-stick capillary blood lactate (*A*), heart rate (HR; *B*), hemoglobin oxygen saturation (StO_2; *C*), total hemoglobin (total[Hb+Mb]; *D*), blood flow index (BF_i; *E*), and tissue regional oxygen metabolic rate (MRO_{2i}; *F*) during the ramp-incremental cycling exercise across normalized power. For each power the last 1.5–2 min of data were averaged. Values are means ± SE. Data points with symbols in common are not significantly different from each other ($P > 0.05$). Black is used for consecutive data points and red for nonconsecutive points.

and MRO_{2i} increased over the interval 15%–75% W_{peak} and then plateaued until the end of the exercise. The BF_i plateau was associated with the rising of the lactate concentration. During the recovery at 15% W_{peak}, BF_i and MRO_{2i} started to decrease (although only MRO_{2i} decreased significantly). The time course of group mean profiles of normalized StO_2, total[Hb+Mb], HR, and MRO_{2i} (Supplemental Fig. S3) confirms the time course of the same parameters reported in the Fig. 5.

Figure 6 illustrates the differences between group average BF at large and short separations. At W_{peak}, the changes of the absolute values of $ssBF_i$ (Fig. 6*A*) were observed ~65% lower than the changes of the absolute values of BF_i (Fig. 4*E*). Figure. 6*B* shows the average across subjects of BF_i and $ssBF_i$ normalized to the max flow rate during exercise.

The two curves are almost superimposable during the exercise, whereas diverge during the recovery phase. In particular, $ssBF_i$ remains almost unchanged, whereas BF_i significantly decreases.

DISCUSSION

Summary of results. In this study, we proposed a new motion correction algorithm for DCS-derived BF_i that is able to remove motion artifacts using an additive term proportional to the pedaling rate. We tested the motion correction algorithm on 18 subjects during cycling exercise and demonstrated for the first time, to the best of our knowledge, that DCS can be used to quantify BF_i continuously during dynamic high-intensity muscle exercise. In addition, we combined DCS with FDNIRS to obtain both hemodynamic and oxygen metabolism measurements of the right superficial rectus femoris during the incremental exercise performed until volitional fatigue.

Comparison with other methods. Over the years, several methods for determining skeletal muscle BF have been developed, allowing for the assessment of global flow to the limbs and more local muscle-specific BF (19).

However, a high-resolution method for the continuous determination of BF at the microcirculatory level in the exercising human skeletal muscle is still lacking. In recent years, a novel optical technique, known as DCS, has been developed. It offers the ability to quantify relative changes in microvascular muscle BF with high speed and accuracy. DCS-derived BF_i has been validated against established muscle perfusion measurement methods, specifically arterial spin labeling MRI (41) and fluorescent microspheres (35). Unfortunately, DCS is highly sensitive to motion artifacts that distort signals coming from the exercising muscle. Very recently, 11 studies carried out on human skeletal muscle, utilizing integrated NIRS/DCS instruments, were reviewed by Hou et al. (27). In most of those studies, BF_i was measured during and/or after cuff occlusion. Only two studies have reported BF_i data during plantar flexion exercise (26, 42) and one during handgrip exercise (21). The algorithms proposed in those studies cannot be adopted for protocols implying dynamic muscle exercises, like cycling. Three recent studies (2, 24, 39) have validated DCS-derived measurements of skeletal muscle BF during rhythmic handgrip exercise comparing DCS with Doppler ultrasound, an established flow imaging modality commonly used to assess skeletal muscles. Bangalore et al. (2) and Tucker et al. (39) were able to measure BF_i during stationary exercise. Furthermore, Hammer et al. (24), using the same instrumentation adopted for the present study and analyzing the BF_i signal only during the 10-s end-stage resting period, found a relative agreement between brachial artery BF (measured by Doppler ultrasound) and BF_i (measured by DCS) only up to ~60%–70% peak power. At this power, BF_i plateaued, whereas brachial artery BF was continuing to increase. All three of these studies have demonstrated a good agreement between DCS and Doppler ultrasound data, both in terms of the magnitude of change and of the temporal relationship. In addition, DCS-derived BF_i was found to be more reliable and less susceptible to artifacts than Doppler ultrasound (2). Although the very recent study by He et al. (25) has demonstrated the possibility to provide absolute cerebral BF measurements by DCS and intermittent intravenous injections of the optical contrast agent indocyanine green, this single-subject calibration procedure is not practical for muscle measurements in the sport settings.

Significance of findings. The noninvasive measure of muscle oxygen consumption is of great interest in exercise physiology (20). It is well known that during exercise, skeletal muscle perfusion increases in direct proportion to the metabolic demand (30). A recent review highlights the formation, interaction, and effect of vasodilator substances that are likely candidates to be important for BF regulation in human skeletal muscle (32). In the present study at the W_{peak}, BF_i increased ~7 times with respect to the pre-exercise level. A very similar BF increase was found at W_{peak} by Calbet et al. (6) during incremental exercise until exhaustion on the cycle ergometer. In that study, femoral venous BF was measured invasively using constant-infusion thermodilution. In the present study, BF_i has plateaued from around 75% W_{peak} through the 15% W_{peak} stage during the recovery phase (Fig. 4), whereas MRO_{2i} has plateaued from around 75% W_{peak} up to 100% W_{peak} and then immediately has started to decrease after the subjects reached their tolerance limit and the bike power setting was decreased to 30 W. The plateaued BF_i was associated with the

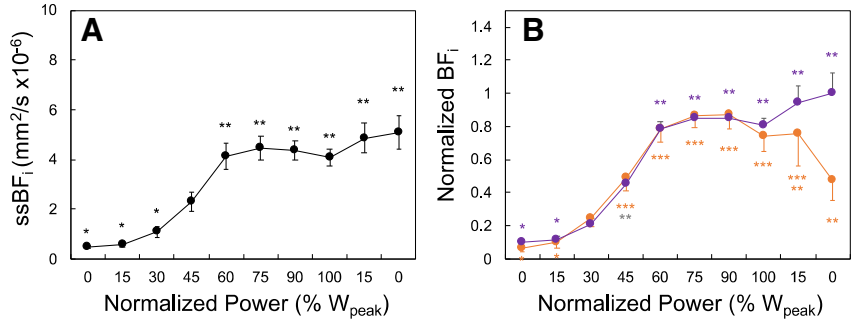

Fig. 6. Group mean profiles of absolute subcutaneous blood flow index ($ssBF_i$; *A*) and normalized muscle (orange) and subcutaneous (purple) BF_i (*B*) during the ramp-incremental cycle exercise across normalized power. Values are means ± SE. Data points with symbols in common are not significantly different from each other ($P > 0.05$). Purple and orange are used for consecutive data points and gray for nonconsecutive points.

well-known rising lactate concentration that indicates a progressive involvement of the anaerobic metabolism. In fact, if the duration of the exercise is sufficient to increase body/core temperature, skin BF increases to facilitate heat loss (30). This is confirmed by the $ssBF_i$ data (Fig. 5). Interestingly, $ssBF_i$ was unchanged during the recovery period, whereas muscle BF_i consistently decreased during the 2-min no-pedaling recovery phase (Fig. 4). The maintenance of a high skin blood flow at the end of cycling exercise is confirmed by a recent study that has utilized laser Doppler flowmetry to provide a qualitative index of skin blood (9).

StO_2 started to decrease at high cycling powers (60% W_{peak}). Deoxy[Hb+Mb] did not plateau toward the end of the ramp-incremental exercise (data not shown). A recent study performed on subjects able to reach a greater W_{peak} (around at 300 W) with respect to the ones in the present study demonstrated that an oxygen extraction reserve still exists in different pools of active muscle fibers of the quadriceps at the end of a ramp exercise to exhaustion (28). The greater magnitude in the reserve was observed in the deeper portion of the vastus lateralis, which is likely due to a greater population of slow-twitch fibers.

Methodological considerations. In the present study, the probe of the commercial system utilized also by Hammer (24) was replaced by a custom-built probe with DCS and FDNIRS fibers colocalized to measure the same tissue with the two modalities. In addition, the multiple DCS source-detector separations allowed us to differentiate subcutaneous from muscle BF. Muscle activation was not measured in the present study; therefore, the temporal activation of the rectus femoris couldn't be determined. The negative motion-corrected BF_i values, observed in some subjects during the recovery phase (Fig. 2), are due to the assumption that BF_i does not change at the onset of the motion. It is plausible that a small increase of BF happens immediately as soon as the subject starts moving. Although we can refine the algorithm by imposing the correction factor to not give negative BF_i values, we plan to optimize the motion correction procedure in future studies by asking the subject to move for few seconds and then stop, then to repeat this a few times at the beginning of the measurements. This will allow us to quantify the constant by imposing that BF_i at the end of the short motion period returns to the initial value.

Limitations. This study has some limitations that are summarized as follows:

1. Testing of the DCS motion artifact compensation algorithm only during cyclic motion.
2. The lack of validation of the DCS motion artifact algorithm by an independent BF measurement. The algorithm could be validated against, for example, the BF measurement obtained by the invasive indocyanine green method and NIRS (22, 40).
3. Empirical model of the motion correction algorithm. This method is strongly dependent of probe location and coupling. Therefore, the calibration needs to be repeated every time the probe is removed and replaced. Smaller artifacts should be obtained by using a wearable DCS instrument.
4. Single local BF_i measurements. The optimal DCS technology should include a multisite system to reveal consistent differences in StO_2 and BF_i, which are expected in the quadriceps muscle groups during ramp-incremental cycle exercise (28, 40).
5. High cost and complexity of the instrumentation. Although this device is a high-end system for research, there are viable solutions to make DCS more affordable and wearable to be easily exploited for muscle physiology applications. The challenges and the future prospective of DCS instrumentations have been recently reviewed (27). Portable inexpensive NIRS/DCS systems utilizing advanced algorithms should be soon widely commercialized for routine utilization (31, 43).
6. Small sample size. The study should be performed on a larger number of subjects to make a consistent interpretation of the BF kinetics.
7. No trained cyclists included in the study. In the present study, only recreationally active subjects were recruited. Therefore, at the end of the protocol, as guided by the Institutional Review Board, the W_{peak}, the lactate concentration, and the HR were not high as in the case of those observable in trained cyclists.
8. No observation of the breakpoint in muscle oxygenation kinetics. Taking into account that in the present study the W_{peak} was overestimated, it is reasonable that it was not possible to observe the deoxy[Hb+Mb] breakpoint that has been observed at the end of a cycling incremental exercise (around 80% W_{peak}) (4, 5). In fact, the true maximal effort would result in a lower relative work rate if scaled to a true maximal effort.
9. Blood lactate measurements. These values are global measurements and may not precisely reflect the superficial rectus femoris anaerobic metabolism.
10. Lack of skin temperature monitoring. Body temperature as well as the local temperature measured on the skin overlying the quadriceps muscle should be monitored in future studies to better investigate the relationship between BF_i and muscle oxidative metabolism during the exercise and the recovery phase.
11. Lack of pulmonary oxygen uptake measurements. For this reason, it was not possible to evaluate the subjects' performances.

Conclusions. These findings further highlight the utility of DCS and FDNIRS oximetry as an effective, reproducible, and noninvasive technique to assess muscle BF_i and MRO_{2i} in real time during a dynamic exercise such as cycling. This paper describes a robust BF correction algorithm for cyclic motion. These results represent important groundwork for future studies aimed at investigating the pathophysiology of microvascular BF and oxidative metabolism relationship during dynamic exercise.

ACKNOWLEDGMENTS

We thank the participants for time and contributions to this study.

GRANTS

This research was sponsored in part by Dynometrics, Inc.

DISCLOSURES

This article reports data acquired with a device from ISS Inc. None of the authors have any financial interests or relation with ISS Inc. D. Wiese owns a company (Dynometrics, Inc.) that makes a device (Humon) that uses continuous-wave NIRS technology for athletes to evaluate muscle performance. P. Anderson at the time of the measurements worked for the company Dynomet-

rics. A. Franceschini, after a study sponsored by Dynometrics was concluded, became an advisory board member of the company (<1% equity). A. Franceschini and S. A. Carp have patents on the FDNIRS and DCS technologies used in this manuscript. A. Franceschini's interests were reviewed and are managed by Massachusetts General Hospital and Partners HealthCare in accordance with their conflict of interest policies. No conflict of interest, financial or otherwise, are declared by the other authors.

AUTHOR CONTRIBUTIONS

P.F., P.A., and M.A.F. conceived and designed research; P.F., P.A., and D.W. performed experiments; V.Q., P.F., and M.A.F. analyzed data; V.Q., P.F., S.A.C., M.F., and M.A.F. interpreted results of experiments; V.Q., P.F., P.Y.F., M.F., and M.A.F. prepared figures; V.Q., P.F., M.F., and M.A.F. drafted manuscript; V.Q., P.F., P.A., P.Y.F., D.W., S.A.C., M.F., and M.A.F. edited and revised manuscript; V.Q., P.F., P.A., P.Y.F., D.W., S.A.C., and M.F. approved final version of manuscript.

REFERENCES

1. **Andresen B, De Carli A, Fumagalli M, Giovannella M, Durduran T, Michael Weigel U, Contini D, Spinelli L, Torricelli A, Greisen G.** Cerebral oxygenation and blood flow in normal term infants at rest measured by a hybrid near-infrared device (BabyLux). *Pediatr Res* 86: 515–521, 2019. doi:10.1038/s41390-019-0474-9.
2. **Bangalore-Yogananda CG, Rosenberry R, Soni S, Liu H, Nelson MD, Tian F.** Concurrent measurement of skeletal muscle blood flow during exercise with diffuse correlation spectroscopy and Doppler ultrasound. *Biomed Opt Express* 9: 131–141, 2017. doi:10.1364/BOE.9.000131.
3. **Barstow TJ.** Understanding near infrared spectroscopy and its application to skeletal muscle research. *J Appl Physiol (1985)* 126: 1360–1376, 2019. doi:10.1152/japplphysiol.00166.2018.
4. **Boone J, Barstow TJ, Celie B, Prieur F, Bourgois J.** The interrelationship between muscle oxygenation, muscle activation, and pulmonary oxygen uptake to incremental ramp exercise: influence of aerobic fitness. *Appl Physiol Nutr Metab* 41: 55–62, 2016. doi:10.1139/apnm-2015-0261.
5. **Boone J, Vandekerckhove K, Coomans I, Prieur F, Bourgois JG.** An integrated view on the oxygenation responses to incremental exercise at the brain, the locomotor and respiratory muscles. *Eur J Appl Physiol* 116: 2085–2102, 2016. doi:10.1007/s00421-016-3468-x.
6. **Calbet JA, Gonzalez-Alonso J, Helge JW, Søndergaard H, Munch-Andersen T, Boushel R, Saltin B.** Cardiac output and leg and arm blood flow during incremental exercise to exhaustion on the cycle ergometer. *J Appl Physiol (1985)* 103: 969–978, 2007. doi:10.1152/japplphysiol.01281.2006.
7. **Carp SA, Farzam P, Redes N, Hueber DM, Franceschini MA.** Combined multi-distance frequency domain and diffuse correlation spectroscopy system with simultaneous data acquisition and real-time analysis. *Biomed Opt Express* 8: 3993–4006, 2017. doi:10.1364/BOE.8.003993.
8. **Chin LM, Kowalchuk JM, Barstow TJ, Kondo N, Amano T, Shiojiri T, Koga S.** The relationship between muscle deoxygenation and activation in different muscles of the quadriceps during cycle ramp exercise. *J Appl Physiol (1985)* 111: 1259–1265, 2011. doi:10.1152/japplphysiol.01216.2010.
9. **Choo HC, Nosaka K, Peiffer JJ, Ihsan M, Yeo CC, Abbiss CR.** Reliability of laser Doppler, near-infrared spectroscopy and Doppler ultrasound for peripheral blood flow measurements during and after exercise in the heat. *J Sports Sci* 35: 1715–1723, 2017. doi:10.1080/02640414.2016.1235790.
10. **Dehaes M, Aggarwal A, Lin PY, Rosa Fortuno C, Fenoglio A, Roche-Labarbe N, Soul JS, Franceschini MA, Grant PE.** Cerebral oxygen metabolism in neonatal hypoxic ischemic encephalopathy during and after therapeutic hypothermia. *J Cereb Blood Flow Metab* 34: 87–94, 2014. doi:10.1038/jcbfm.2013.165.
11. **Durduran T, Choe R, Baker WB, Yodh AG.** Diffuse optics for tissue monitoring and tomography. *Rep Prog Phys* 73: 076701, 2010. doi:10.1088/0034-4885/73/7/076701.
12. **Durduran T, Yodh AG.** Diffuse correlation spectroscopy for non-invasive, micro-vascular cerebral blood flow measurement. *Neuroimage* 85: 51–63, 2014. doi:10.1016/j.neuroimage.2013.06.017.
13. **Farzam P, Buckley EM, Lin PY, Hagan K, Grant PE, Inder TE, Carp SA, Franceschini MA.** Shedding light on the neonatal brain: probing cerebral hemodynamics by diffuse optical spectroscopic methods. *Sci Rep* 7: 15786, 2017. [Erratum in *Sci Rep* 7:15786, 2017.] doi:10.1038/s41598-017-15995-1.
14. **Farzam P, Durduran T.** Multidistance diffuse correlation spectroscopy for simultaneous estimation of blood flow index and optical properties. *J Biomed Opt* 20: 55001, 2015. doi:10.1117/1.JBO.20.5.055001.
15. **Farzam P, Starkweather Z, Franceschini MA.** Validation of a novel wearable, wireless technology to estimate oxygen levels and lactate threshold power in the exercising muscle. *Physiol Rep* 6: e13664, 2018. doi:10.14814/phy2.13664.
16. **Ferradal SL, Yuki K, Vyas R, Ha CG, Yi F, Stopp C, Wypij D, Cheng HH, Newburger JW, Kaza AK, Franceschini MA, Kussman BD, Grant PE.** Non-invasive assessment of cerebral blood flow and oxygen metabolism in neonates during hypothermic cardiopulmonary bypass: Feasibility and clinical implications. *Sci Rep* 7: 44117, 2017. doi:10.1038/srep44117.
17. **Ferrari M, Muthalib M, Quaresima V.** The use of near-infrared spectroscopy in understanding skeletal muscle physiology: recent developments. *Philos Trans A Math Phys Eng Sci* 369: 4577–4590, 2011. doi:10.1098/rsta.2011.0230.
18. **Giovannella M, Contini D, Pagliazzi M, Pifferi A, Spinelli L, Erdmann R, Donat R, Rocchetti I, Rehberger M, König N, Schmitt R, Torricelli A, Durduran T, Weigel UM.** BabyLux device: a diffuse optical system integrating diffuse correlation spectroscopy and time-resolved near-infrared spectroscopy for the neuromonitoring of the premature newborn brain. *Neurophotonics* 6: 025007, 2019. doi:10.1117/1.NPh.6.2.025007.
19. **Gliemann L, Mortensen SP, Hellsten Y.** Methods for the determination of skeletal muscle blood flow: development, strengths and limitations. *Eur J Appl Physiol* 118: 1081–1094, 2018. doi:10.1007/s00421-018-3880-5.
20. **Grassi B, Quaresima V.** Near-infrared spectroscopy and skeletal muscle oxidative function in vivo in health and disease: a review from an exercise physiology perspective. *J Biomed Opt* 21: 091313, 2016. doi:10.1117/1.JBO.21.9.091313.
21. **Gurley K, Shang Y, Yu G.** Noninvasive optical quantification of absolute blood flow, blood oxygenation, and oxygen consumption rate in exercising skeletal muscle. *J Biomed Opt* 17: 075010, 2012. doi:10.1117/1.JBO.17.7.075010.
22. **Habazettl H, Athanasopoulos D, Kuebler WM, Wagner H, Roussos C, Wagner PD, Ungruhe J, Zakynthinos S, Vogiatzis I.** Near-infrared spectroscopy and indocyanine green derived blood flow index for noninvasive measurement of muscle perfusion during exercise. *J Appl Physiol (1985)* 108: 962–967, 2010. doi:10.1152/japplphysiol.01269.2009.
23. **Hamaoka T, McCully KK, Niwayama M, Chance B.** The use of muscle near-infrared spectroscopy in sport, health and medical sciences: recent developments. *Philos Trans A Math Phys Eng Sci* 369: 4591–4604, 2011. doi:10.1098/rsta.2011.0298.
24. **Hammer SM, Alexander AM, Didier KD, Smith JR, Caldwell JT, Sutterfield SL, Ade CJ, Barstow TJ.** The noninvasive simultaneous measurement of tissue oxygenation and microvascular hemodynamics during incremental handgrip exercise. *J Appl Physiol (1985)* 124: 604–614, 2018. doi:10.1152/japplphysiol.00815.2017.
25. **He L, Baker WB, Milej D, Kavuri VC, Mesquita RC, Busch DR, Abramson K, Jiang JY, Diop M, St Lawrence K, Amendolia O, Quattrone F, Balu R, Kofke WA, Yodh AG.** Noninvasive continuous optical monitoring of absolute cerebral blood flow in critically ill adults. *Neurophotonics* 5: 045006, 2018. doi:10.1117/1.NPh.5.4.045006.
26. **Henry B, Zhao M, Shang Y, Uhl T, Thomas DT, Xenos ES, Saha SP, Yu G.** Hybrid diffuse optical techniques for continuous hemodynamic measurement in gastrocnemius during plantar flexion exercise. *J Biomed Opt* 20: 125006, 2015. doi:10.1117/1.JBO.20.12.125006.
27. **Hou L, Liu Y, Qian L, Zheng Y, Gao J, Cao W, Shang Y.** Portable near-infrared technologies and devices for noninvasive assessment of tissue hemodynamics. *J Healthc Eng* 2019: 3750495, 2019. doi:10.1155/2019/3750495.
28. **Iannetta D, Okushima D, Inglis EC, Kondo N, Murias JM, Koga S.** Blood flow occlusion-related O_2 extraction "reserve" is present in different muscles of the quadriceps but greater in deeper regions after ramp-incremental test. *J Appl Physiol (1985)* 125: 313–319, 2018. doi:10.1152/japplphysiol.00154.2018.
29. **Lai N, Zhou H, Saidel GM, Wolf M, McCully K, Gladden LB, Cabrera ME.** Modeling oxygenation in venous blood and skeletal muscle in response to exercise using near-infrared spectroscopy. *J Appl Physiol (1985)* 106: 1858–1874, 2009. doi:10.1152/japplphysiol.91102.2008.
30. **Laughlin MH, Davis MJ, Secher NH, van Lieshout JJ, Arce-Esquivel AA, Simmons GH, Bender SB, Padilla J, Bache RJ, Merkus D, Duncker DJ.** Peripheral circulation. *Compr Physiol* 2: 321–447, 2012. doi:10.1002/cphy.c100048.

31. **Li T, Lin Y, Shang Y, He L, Huang C, Szabunio M, Yu G.** Simultaneous measurement of deep tissue blood flow and oxygenation using noncontact diffuse correlation spectroscopy flow-oximeter. *Sci Rep* 3: 1358, 2013. doi:10.1038/srep01358.
32. **Mortensen SP, Saltin B.** Regulation of the skeletal muscle blood flow in humans. *Exp Physiol* 99: 1552–1558, 2014. doi:10.1113/expphysiol.2014.081620.
33. **Okushima D, Poole DC, Barstow TJ, Rossiter HB, Kondo N, Bowen TS, Amano T, Koga S.** Greater $\dot{V}O2$peak is correlated with greater skeletal muscle deoxygenation amplitude and hemoglobin concentration within individual muscles during ramp-incremental cycle exercise. *Physiol Rep* 4: e13065, 2016. doi:10.14814/phy2.13065.
34. **Perrey S, Ferrari M.** Muscle oximetry in sports science: a systematic review. *Sports Med* 48: 597–616, 2018. doi:10.1007/s40279-017-0820-1.
35. **Proctor AR, Ramirez GA, Han S, Liu Z, Bubel TM, Choe R.** Validation of diffuse correlation spectroscopy sensitivity to nicotinamide-induced blood flow elevation in the murine hindlimb using the fluorescent microsphere technique. *J Biomed Opt* 23: 1–9, 2018. doi:10.1117/1.JBO.23.3.035006.
36. **Roche-Labarbe N, Carp SA, Surova A, Patel M, Boas DA, Grant PE, Franceschini MA.** Noninvasive optical measures of CBV, StO(2), CBF index, and rCMRO(2) in human premature neonates' brains in the first six weeks of life. *Hum Brain Mapp* 31: 341–352, 2010. doi:10.1002/hbm.20868.
37. **Shang Y, Li T, Yu G.** Clinical applications of near-infrared diffuse correlation spectroscopy and tomography for tissue blood flow monitoring and imaging. *Physiol Meas* 38: R1–R26, 2017. doi:10.1088/1361-6579/aa60b7.
38. **Shang Y, Symons TB, Durduran T, Yodh AG, Yu G.** Effects of muscle fiber motion on diffuse correlation spectroscopy blood flow measurements during exercise. *Biomed Opt Express* 1: 500–511, 2010. doi:10.1364/BOE.1.000500.
39. **Tucker WJ, Rosenberry R, Trojacek D, Chamseddine HH, Arena-Marshall CA, Zhu Y, Wang J, Kellawan JM, Haykowsky MJ, Tian F, Nelson MD.** Studies into the determinants of skeletal muscle oxygen consumption: novel insight from near-infrared diffuse correlation spectroscopy. *J Physiol* 597: 2887–2901, 2019. doi:10.1113/JP277580.
40. **Vogiatzis I, Habazettl H, Louvaris Z, Andrianopoulos V, Wagner H, Zakynthinos S, Wagner PD.** A method for assessing heterogeneity of blood flow and metabolism in exercising normal human muscle by near-infrared spectroscopy. *J Appl Physiol (1985)* 118: 783–793, 2015. doi:10.1152/japplphysiol.00458.2014.
41. **Yu G, Floyd TF, Durduran T, Zhou C, Wang J, Detre JA, Yodh AG.** Validation of diffuse correlation spectroscopy for muscle blood flow with concurrent arterial spin labeled perfusion MRI. *Opt Express* 15: 1064–1075, 2007. doi:10.1364/OE.15.001064.
42. **Yu G, Durduran T, Lech G, Zhou C, Chance B, Mohler ER III, Yodh AG.** Time-dependent blood flow and oxygenation in human skeletal muscles measured with noninvasive near-infrared diffuse optical spectroscopies. *J Biomed Opt* 10: 024027, 2005. doi:10.1117/1.1884603.
43. **Zhang P, Gui Z, Guo G, Shang Y.** Approaches to denoise the diffuse optical signals for tissue blood flow measurement. *Biomed Opt Express* 9: 6170–6185, 2018. doi:10.1364/BOE.9.006170.